J. Appl. Cryst. (1996). **29**, 411–418

Electron Diffraction Patterns of Fibrous and Lamellar Textured Polycrystalline Thin Films. I. Theory

L. TANG AND D. E. LAUGHLIN

Data Storage Systems Center, Department of Materials Science and Engineering, Carnegie Mellon University, Pittsburgh, PA 15213, USA

(*Received 20 October 1995; accepted 8 January 1996*)

Abstract

The reciprocal lattices of fibrous and lamellar textured polycrystalline thin films are analyzed on the basis of the number of distinct angles made between planes of {*hkl*} families with the texture axis. Tables of the maximum possible number of such distinct angles between any given direction/plane and all faces of a given family of planes for all the crystal systems are included in this paper. Based on these reciprocal lattices, parallel and tilted electron-diffraction-pattern characteristics of the textured films are elucidated. A method of indexing the arced electron diffraction patterns of the textured films is proposed. This method can be applied to both the fibrous and lamellar texture films of all crystal structures. Formulas that relate the angles subtended by diffraction arcs to the distribution angle of the texture axis are presented.

1. Introduction

When materials are sputtered onto a substrate they often form polycrystalline thin films in which the grains have preferred orientation. Such thin films are said to be crystallographically textured. The texture of thin films can be divided into two distinct categories, namely fibrous texture and lamellar texture (Vainshtein, 1964; Zvyagin, 1992; Hirsch, Howie, Nicholson, Pashley & Whelan, 1978; Reimer, 1984). In fibrous texture, many of the individual grains of the film have a particular crystallographic direction that is parallel to a specific reference direction, which is termed the fiber direction. In lamellar texture, a certain set of crystallographic planes is parallel to a specified reference plane. For thin films, the reference direction for fibrous texture is usually the normal to the film, whereas the reference plane for lamellar texture is usually the plane of the thin film, which is parallel to the substrate on which the thin film grew. In this paper, our emphasis will be on the investigation of fibrous and lamellar textures of thin films.

Most treatments of crystallographic texture are done for the texture of bulk materials (Barrett & Massalski, 1980). For this reason, most descriptions of crystallographic texture have been written with X-ray diffraction techniques in mind. In this paper, we discuss the analysis of the texture of thin films from transmission electron diffraction patterns.

The textures of thin films have been studied by various diffraction techniques. For example, X-ray diffraction techniques with different geometric arrangements, such as symmetric and asymmetric scans, rocking scans, and pole figures, are frequently used for texture studies of thin films (Cullity, 1978; Bain, Clemens, Brennan & Kataoka, 1993; Feng, Laughlin & Lambeth, 1994). However, since the thickness of the films is often of 10–100 nm, these techniques do not always produce reliable results. This is due to either the strong background signal from the substrate of single-layer films or overlapping of diffraction peaks of the different layers for multilayered films. In addition, information about the grain size and other microstructural features, such as defects and elemental segregation, of the films is usually not easily obtained by X-ray diffraction techniques.

In this paper, we present a unified treatment of the analysis of fibrous and lamellar textured thin films as investigated by transmission electron diffraction patterns. Such patterns can be obtained from films of the order of 10–100 nm thick and the direct-space structure of the film can be easily obtained from the same area from which the diffraction patterns are obtained. The diffraction patterns can be approximated as sections through the intensity-weighted reciprocal lattice. An example of a series of electron diffraction patterns taken from a textured body-centered-cubic (b.c.c.) Cr ($a = 2.885$ Å) thin film is shown in Fig. 1. The pattern with uniform rings in Fig. 1(*a*) is the one when the texture axis is parallel to the electron beam. Some of the rings that would appear in the randomly oriented films are missing in this pattern. Hono, Wong & Laughlin (1990) have developed tables for the determination of the intensities of the various *hkl* rings relative to each other for various textures of b.c.c. Cr and hexagonal-close-packed (h.c.p.) Co thin films. More information can however be obtained from the diffraction patterns taken when the texture axis is tilted away about an axis **OT** in the film plane from the electron beam (Figs. 1*b–h*). The patterns can be seen to undergo a complicated evolution producing arced

electron diffraction patterns. These arced diffraction patterns have been used in determining the indices of the texture axis (Vainshtein, 1964; Zvyagin, 1992; Hirsch *et al.*, 1978; Reimer, 1984; Tang & Thomas, 1993).

Herein we develop equations that can be utilized to more fully analyze the arced electron diffraction patterns. In particular, it will be shown that the distribution angle, α, of the texture axis can be determined by systematic tilting experiments. Our approach is different from the previous work (Vainshtein, 1964; Zvyagin, 1992) in that we treat fibrous and lamellar textures in a unified way. In a second paper, we will illustrate the use of the methods developed herein with examples from thin films of various crystal structures.

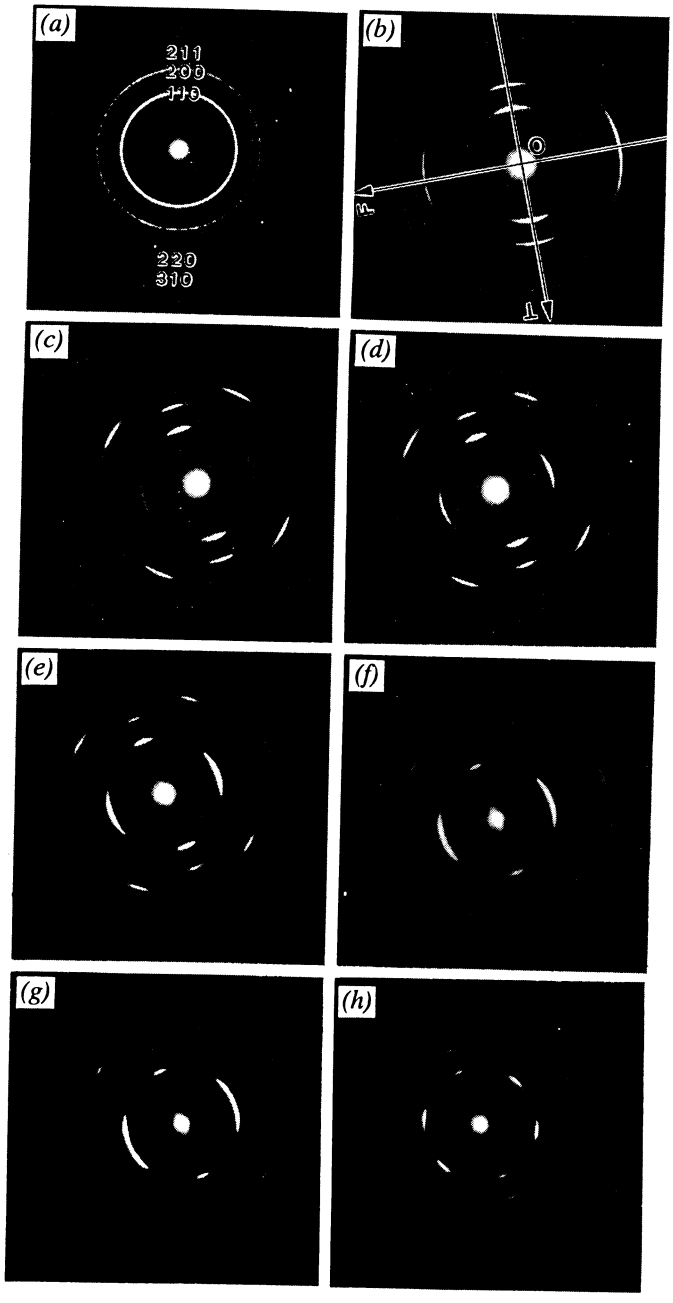

Fig. 1. Electron diffraction patterns of a textured b.c.c. Cr film at (*a*) 0, (*b*) 21, (*c*) 38, (*d*) 43, (*e*) 45, (*f*) 47, (*g*) 49 and (*h*) 55° tilt.

2. Reciprocal lattice of textured polycrystalline thin films

2.1. *Fibrous texture*

Polycrystalline samples with grains having a common crystallographic direction $\mathbf{R} = u\mathbf{a} + v\mathbf{b} + w\mathbf{c} = [uvw]$ parallel to a reference direction (while other crystallographic directions are randomly oriented around this reference direction) are said to have a fibrous texture. Here, u, v and w are integers and are coprime and **a**, **b** and **c** are the unit-cell vectors of the real-space lattice. For thin films, the reference direction is usually the normal to the plane of the substrate. The reciprocal lattice of a fibrous textured polycrystalline sample is equivalent to that of a single crystal with all of the reciprocal-lattice points rotated around the fiber axis $[uvw]$ (Vainshtein, 1964; Hirsch *et al.*, 1978; Reimer, 1984). Thus, each hkl reciprocal-lattice point becomes a reciprocal circle around $[uvw]$. For an $\{hkl\}$ family in which there are P (multiplicity factor) lattice planes with the same d spacing and structure factor, the corresponding reciprocal-lattice circles are circles with different latitudes on a sphere with $[uvw]$ as the **NS** direction (Fig. 2). The radius of the sphere is $G_{\{hkl\}} = (\mathbf{G}_{\{hkl\}} \cdot \mathbf{G}_{\{hkl\}})^{1/2} = 1/d_{hkl}$, where $\mathbf{G}_{\{hkl\}}$ is the set of all the P reciprocal-lattice vectors of $\{hkl\}$. Because some planes in the $\{hkl\}$ family may have the same angle, ρ, with respect to $[uvw]$, the number of the $\{hkl\}$ reciprocal circles may not be equal to P, but is the number of distinct angles, N, between the normals to the $\{hkl\}$ planes and $[uvw]$. Tables 1–5 list the maximum possible number of distinct angles, $M \leq P$, between any given crystallographic direction $[uvw]$ and/or plane $(h'k'l')$ and all planes in a given family of planes in cubic

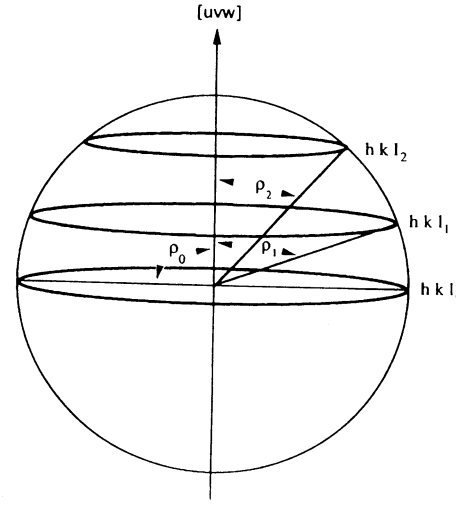

Fig. 2. Reciprocal circles of an $\{hkl\}$ family of planes making three distinct angles with the fiber texture axis $[uvw]$.

Table 1. *Maximum number of distinct angles between any given direction/plane and all faces of a given plane family in the cubic system*

A number with an asterisk indicates that one of the angles is equal to 90°.

Direction	*uvw*	*uuw*	0*vw*	110	111	001
Plane	*h'k'l'*	*h'h'l'*	0*k'l'*	110	111	001
Plane family (*P*)						
hkl (24)	24	12	12	6	4	3
hhl (12)	12	7	6	4*	3	2
0*kl* (12)	12	6	8	4	2	3*
0*kk* (6)	6	4*	4	3*	2*	2*
hhh (4)	4	3	2	2*	2	1
00*l* (3)	3	2	3*	2*	1	2*

Table 2. *Maximum number of distinct angles between any given direction/plane and all the faces of a given plane family in the tetragonal system*

A number with an asterisk indicates that one of the angles is equal to 90°.

Direction	*uvw*	*uuw*	0*vw*	*uv*0	110	010	001
Plane	*h'k'l'*	*h'h'l'*	0*k'l'*	*h'k'*0	110	010	001
Plane family (*P*)							
hkl (8)	8	4	4	4	2	2	1
hhl (4)	4	2	2	2	2*	1	1
0*kl* (4)	4	2	2	2	1	2*	1
*hk*0 (4)	4	2	2	2	2	2	1*
*hh*0 (2)	2	2*	1	2	2*	1	1*
0*k*0 (2)	2	1	2*	2	1	2*	1*
00*l* (1)	1	1	1	1*	1*	1*	1

(Kasper & Lonsdale, 1959), tetragonal, orthorhombic, hexagonal and monoclinic crystal systems. In these tables, no distinction is made between $\{hkl\}$ and $\{\bar{h}\bar{k}\bar{l}\}$ and a number with an asterisk indicates that one of the angles is equal to 90°. Values of the angles can be calculated by

$$\cos\rho_i = \mathbf{R}\cdot\mathbf{G}_{\{hkl\}_i}/RG_{\{hkl\}} = (h_iu + k_iv + l_iw)/RG_{\{hkl\}}$$
$$= n_i/RG_{\{hkl\}}$$
$$(n_i = \text{integer}, i = 0, 1, 2, \ldots, N-1 \le M-1 \quad \text{or}$$
$$i = 1, 2, \ldots, N \le M), \qquad (1)$$

where $h_i\mathbf{a}^* + k_i\mathbf{b}^* + l_i\mathbf{c}^*$ is one of the reciprocal-lattice vectors in $\mathbf{G}_{\{hkl\}_i}$ which includes those reciprocal vectors in $\mathbf{G}_{\{hkl\}}$, making the same angle, ρ_i, with $\mathbf{R}$. It should be noted that possible values of n are fixed once $[uvw]$ is fixed for a given crystal system. With the help of (1), reciprocal-lattice circles of an $\{hkl\}$ family with N distinct angles with $[uvw]$ can be indexed as hkl_i with i increasing in the order of decreasing values of ρ, where $i = 0, 1, 2, \ldots, N-1 \le M-1$ for $\{hkl\}$, in which there is at least one plane making 90° with $[uvw]$ (Fig. 2) and $i = 1, 2, \ldots, N \le M$ for $\{hkl\}$, in which there are no planes making 90° with $[uvw]$.

This method of indexing the reciprocal circles can be easily seen by means of an example. In a cubic lattice, there are twelve {211} planes, but these twelve {211} planes make only two distinct angles with the [001] direction (see Table 1). Therefore, in a [001] textured film, there are two 211 reciprocal circles about the [001] axis: 211_1, which includes the planes (211), $(\bar{2}11)$, $(2\bar{1}1)$, $(\bar{2}\bar{1}1)$, (121), $(\bar{1}21)$, $(1\bar{2}1)$ and $(\bar{1}\bar{2}1)$, and 211_2, which includes the planes (112), $(\bar{1}12)$, $(1\bar{1}2)$ and $(\bar{1}\bar{1}2)$. The angle ρ_1 is 65.9° and ρ_2 is 35.3° (see Fig. 3). These angles are independent of the lattice parameters of the cubic systems. Notice that there is no {211} plane that is 90° to the [001].

Table 3. *Maximum number of distinct angles between any given direction/plane and all the faces of a given plane family in the orthorhombic system*

A number with an asterisk indicates that one of the angles is equal to 90°.

Direction	*uvw*	0*vw*	*u*0*w*	*uv*0	100	010	001
Plane	*h'k'l'*	0*k'k'*	*h'*0*l'*	*h'k'*0	100	010	001
Plane family (*P*)							
hkl (4)	4	2	2	2	1	1	1
0*kl* (2)	2	2	1	1	1*	1	1
*h*0*l* (2)	2	1	2	1	1	1*	1
*hk*0 (2)	2	1	1	2	1	1	1*
*h*00 (1)	1	1*	1	1	1	1*	1*
0*k*0 (1)	1	1	1*	1	1*	1	1*
00*l* (1)	1	1	1	1*	1*	1*	1

Table 4. *Maximum number of distinct angles between any given direction/plane and all the faces of a given plane family in the hexagonal system*

A number with an asterisk indicates that one of the angles is equal to 90°.

Direction	*uv.w*	*uu.w*	0*v.w*	*uv*.0	11.0	01.0	001.
Plane	*h'k'.l'*	*h'h'.l'*	0*k'.l'*	*h'k'*.0	11.0	01.0	00.1
Plane family (*P*)							
hk.l (12)	12	6	6	6	3	3	1
hh.l (6)	6	4	3	3	2	2*	1
0*k.l* (6)	6	3	4	3	2*	2	1
hk.0 (6)	6	3	3	3	3	3	1*
hh.0 (3)	3	2	2*	3	2	2*	1*
0*k*.0 (3)	3	2*	2	3	2*	2	1*
00.*l* (1)	1	1	1	1*	1*	1*	1

Table 5. *Maximum number of distinct angles between any given direction/plane and all the faces of a given plane family in the monoclinic system*

A number with an asterisk indicates that one of the angles is equal to 90°.

Direction	*uvw*	*u*0*w*	0*v*0
Plane	*h'k'l'*	*h'*0*l'*	0*k'*0
Plane family (*P*)			
hkl (2)	2	1	1
*h*0*l* (1)	1	1	1*
0*k*0 (1)	1	1*	1

In addition, since a crystallographic direction $[uvw]$ in a real lattice is always parallel to the normal to a set of reciprocal-lattice planes $(uvw)^*$ of spacing $1/R$, all the reciprocal circles of different $\{hkl\}$ families must lie on these reciprocal-lattice planes. Furthermore, because the projection of the $\mathbf{G}_{\{hkl\}_i}$ along $[uvw]$ is

$$G_{\{hkl\}} \cos \rho_i = n_i/R, \tag{2}$$

reciprocal circles of different $\{hkl\}$ families but with the same n_i value will lie on the same layer of $(uvw)^*$ reciprocal-lattice planes.

2.2. *Lamellar texture*

Thin films that have grains with a common crystallographic plane $(h'k'l')$ parallel to a reference surface but randomly arranged in the reference surface are described as having a lamellar (or plate) texture (Vainshtein, 1964; Zvyagin, 1992). The reference surface is normally the substrate surface. Therefore, all grains have their $(h'k'l')$ plane normal direction $\mathbf{G}_{h'k'l'} = h'\mathbf{a}^* + k'\mathbf{b}^* + l'\mathbf{c}^* = [h'k'l']^*$ parallel to the normal to the reference surface. Thus, we can define the direction $[h'k'l']^*$ in reciprocal space as the lamellar texture axis. Therefore, just as in the fibrous texture case, all reciprocal-lattice points become circles around the axis $[h'k'l']^*$. It should be noted, however, that $[h'k'l']^*$ is a reciprocal-lattice vector itself and, unlike the real-space crystallographic lattice vector $[uvw]$, may not be the normal to a set of reciprocal-lattice planes, since its directional indices $[u'v'w']$ in the real space may not be integers. For planes in an $\{hkl\}$ family, distinct angles between their reciprocal circles and the $[h'k'l']^*$ direction can be obtained by

$$\cos \varphi_i = \mathbf{G}_{h'k'l'} \cdot \mathbf{G}_{\{hkl\}_i} / (G_{h'k'l'} G_{\{hkl\}}). \tag{3}$$

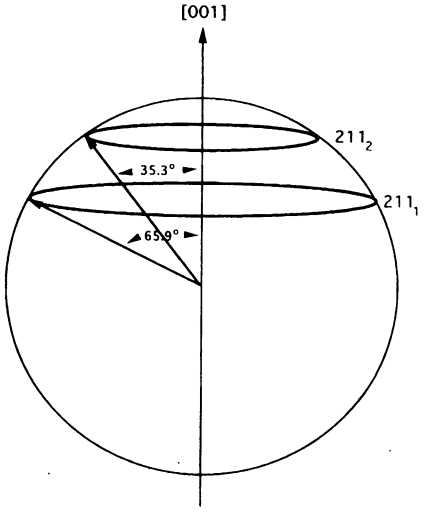

Fig. 3. 211 reciprocal circles of a [001] textured cubic film.

It should be noted that, although (3) usually cannot be simplified to the form $(h'h_i + k'k_i + l'l_i)/C$ where $h'h_i + k'k_l + l'l_i =$ integer and C is a constant, it can always be written in the following form:

$$\cos \varphi_i = (h_i u' + k_i v' + l_i w')/C', \tag{4}$$

where $u'\mathbf{a} + v'\mathbf{b} + w'\mathbf{c} = h'\mathbf{a}^* + k'\mathbf{b}^* + l'\mathbf{c}^*$, $[h_i k_i l_i]^*$ is one of the reciprocal vectors in $\mathbf{G}_{\{hkl\}_i}$ and C' is a constant. u', v' and w' can be obtained by

$$\begin{pmatrix} u' \\ v' \\ w' \end{pmatrix} = \begin{pmatrix} \mathbf{a}^* \cdot \mathbf{a}' & \mathbf{b}^* \cdot \mathbf{a}^* & \mathbf{c}^* \cdot \mathbf{a}^* \\ \mathbf{a}^* \cdot \mathbf{b}^* & \mathbf{b}^* \cdot \mathbf{b}^* & \mathbf{c}^* \cdot \mathbf{b}^* \\ \mathbf{a}^* \cdot \mathbf{c}^* & \mathbf{b}^* \cdot \mathbf{c}^* & \mathbf{c}^* \cdot \mathbf{c}^* \end{pmatrix} \begin{pmatrix} h' \\ k' \\ l' \end{pmatrix}. \tag{5}$$

For cubic systems, (4) reduces to (1), since $[u'v'w'] = [h'k'l']$. Thus, there is no need to distinguish between fibrous and lamellar textures in cubic systems because they have identical reciprocal lattices. For noncubic crystal systems, u', v' and w' need not be integers and thus $hu' + kv' + lw'$ in general is not an integer. Although the angle values may be different, the maximum possible number of distinct angles, M, between the reciprocal circles in $\{hkl\}$ and $[h'k'l']^*$ is the same of that between the reciprocal circles in $\{hkl\}$ and $[uvw]$ if $h' = u$, $k' = v$ and $l' = w$, because (4) and (2) have similar form. Thus, Tables 1–5 apply not only to the fibrous texture but also to the lamellar texture. Similar to the fibrous texture case, reciprocal circles of an $\{hkl\}$ family with different angles with $[h'k'l']^*$ can be indexed as hkl_i and i increases in the order of decreasing values of the angle φ, where $i = 0, 1, 2, 3, \ldots, N - 1 \leq M - 1$ for $\{hkl\}$, in which at least one plane makes 90° with $[h'k'l']^*$, and $i = 1, 2, 3, \ldots, N \leq M$ for $\{hkl\}$, in which there are no planes making 90° with $[h'k'l']^*$. For example, since the number of distinct angles between the six planes in $\{10\bar{1}1\}$ and $(10\bar{1}1)$ is four (see Table 4) for hexagonal lattices, there are four $\{10\bar{1}1\}$ reciprocal circles around the $[10\bar{1}1]^*$ axis in the reciprocal lattice of a $(10\bar{1}1)$ textured film. These four reciprocal circles can be indexed, in order of decreasing angle values, as $10\bar{1}1_1$ including $(01\bar{1}\bar{1})$ and $(1\bar{1}0\bar{1})$, $10\bar{1}1_2$ including $(10\bar{1}\bar{1})$, $10\bar{1}1_3$ including $(1\bar{1}01)$ and $(01\bar{1}1)$ and $10\bar{1}1_4$ including $(10\bar{1}1)$. It is worth pointing out that each of the four circles lies on the sphere of radius $G_{\{10\bar{1}1\}}$ and that values of the angles are dependent on the c/a ratios. Fig. 4 shows the projections on the plane of the reciprocal-lattice circles of $\{10\bar{1}1\}$ planes of a $[10\bar{1}1]^*$ textured hexagonal cobalt film ($a = 2.507$, $c = 4.070$ Å; Cullity, 1978).

2.3. *Effects of film thickness and texture axis distribution angle on the reciprocal lattices of textured thin films*

The finite thickness of single-crystal thin films, t, changes the reciprocal-lattice points into reciprocal-lattice rods of length $2/t$ along the direction of the film thickness. Similarly, reciprocal-lattice circles of textured

thin films become cylindrical belts of height $2/t$. The angle subtended by the cylinders is:

$$\gamma_{hkl} = \tan^{-1}(d_{hkl}/t). \quad (6)$$

Note that this angle decreases for the higher-order reciprocal circles. For example, $\gamma_{110} = 1.2°$ and $\gamma_{200} = 0.8°$ for a 10 nm-thick b.c.c. Cr film. On the other hand, if the texture axis is distributed in an angular interval α around the reference direction, the reciprocal-lattice circles become spherical belts subtending an angle of 2α from the origin. It should be noted that 2α is the same for all of the reciprocal spherical belts while γ_{hkl} varies with d_{hkl}.

3. Characteristics of electron diffraction patterns of textured polycrystalline thin films

Geometrically, electron diffraction patterns of crystals can be approximated as sections of the reciprocal lattice since the reflection or Ewald sphere can be regarded as a plane for high-energy electrons (*i.e.* the radius of the Ewald sphere, $1/\lambda$, is much larger than the lengths of low-index reciprocal-lattice vectors). As discussed in the preceding sections, reciprocal lattices of a $[uvw]$ fibrous and an $[h'k'l']^*$ lamellar textured thin film are similar in that an $\{hkl\}$ family has the same maximum number of distinct reciprocal circles about $[uvw]$ and $[h'k'l']^*$ if $u = h'$, $v = k'$, $w = l'$. Thus, it can be expected that their electron diffraction patterns also will have similar aspects. This enables us to discuss the geometric features of electron diffraction patterns from either fibrous or lamellar textured thin films by the same approach.

3.1. *Electron beam parallel to the fibrous texture axis [uvw] or lamellar texture axis [hkl]**

When the incident electron beam is parallel to the texture axis, the electron diffraction pattern consists of

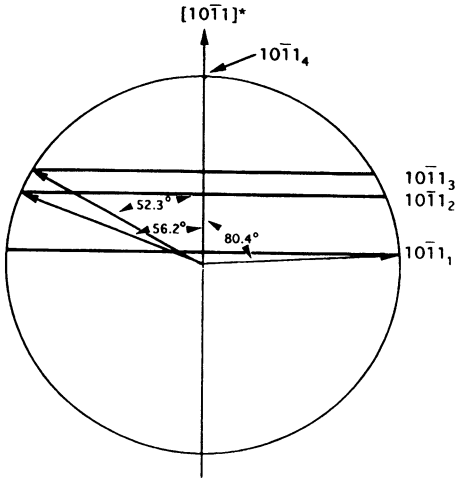

Fig. 4. Projections of 10$\bar{1}$1 reciprocal circles of a [10$\bar{1}$1]* lamellar textured h.c.p. Co film.

hkl_0 rings. Hereinafter we call these patterns *parallel patterns*. These hkl_0 rings satisfy the conditions

$$hu + kv + lw = 0 \quad \text{for fibrous texture;} \quad (7)$$

$$hu' + kv' + lw' = 0 \quad \text{for lamellar texture.} \quad (8)$$

If the crystal structure of the film is known, the indices of each ring can be determined using

$$L\lambda = r_{hkl}d_{hkl}, \quad (9)$$

where $L\lambda$ is the camera constant, r_{hkl} is the radius of the ring and d_{hkl} is the interplanar spacing of the $\{hkl\}$ planes. Indices of $[uvw]$ and $[h'k'l']^*$ can then be determined using (7) and (8) if there are three or more indexed hkl_0 rings. For the fibrous texture, this can always be done, since there must be a $(uvw)^*$ reciprocal plane passing through the origin of the reciprocal lattice and normal to $[uvw]$. For a given $[h'k'l']^*$ or $[u'v'w']$ lamellar texture, it is often possible that there are no (hkl) planes satisfying the condition $hu' + kv' + lw' = 0$ and only the transmitted spot is observed. In order to determine the indices of $[hkl]^*$ for the lamellar texture, diffraction patterns taken with $[h'k'l']^*$ tilted away from the incident electron beam by a certain angle around an axis in the $(h'k'l')$ plane are needed. This is discussed in detail in the next section.

3.2. *[uvw] and [hkl]* tilted away from the incident beam around an axis in the film plane*

When the $[uvw]$ or $[h'k'l']^*$ directions are tilted away from the incident electron beam about an axis in the plane to which the texture axis is normal, the diffraction patterns are no longer uniform rings but are arcs owing to the intersection of the Ewald sphere with the inclined reciprocal spherical belts. We define such patterns as *tilted patterns*. The appearance of the tilted pattern is dependent on the tilt angle β ($\beta = 0°$ corresponds to the parallel pattern). Fig. 5 shows schematically the diffraction pattern evolution due to diffraction of planes of an $\{hkl\}$ family with the tilt angle β. Here, we assume that the $\{hkl\}$ planes have two distinct angles in which one is 90° and the other is η_1 ($\eta_1 = \rho_1$ for fibrous texture and $\eta_1 = \varphi_1$ for lamellar texture) with the texture axis. Thus, there are two reciprocal spherical belts (with $\alpha \gg \gamma$ assumed), hkl_0 and hkl_1, around the texture axis.

First, let us look at the evolution of the hkl_0 ring as the film is being tilted. The hkl_0 ring (Fig. 5*a*) becomes two arcs (Fig. 5*b*) when the tilt angle β is greater than the distribution angle, α, of the texture axis. These two arcs are bisected by the tilt axis **OT** and are symmetric about the transmitted spot. The angle ω_0 subtended by the hkl_0 arcs is not a constant but a function of the tilt angle β and the texture axis distribution angle α. This can be seen from Fig. 6, which shows schematically the intersection of the Ewald sphere with an hkl_0 spherical belt when $\beta > \alpha$. In Fig. 6, **ON** is the direction of the texture axis ($[uvw]$ for fibrous texture and $[h'k'l']^*$ for lamellar

texture), **OE** is the incident electron beam direction, **OT** is the tilt axis, ω_0 is the angle subtended by the hkl_0 arcs with the chord JK bisected by **OT** and LK is the chord of the angle 2α. From the triangle OJK ($OJ = OK = G_{\{hkl\}}$) in Fig. 6, it follows that

$$\sin(\omega_0/2) = JK/2OK. \tag{10}$$

Similarly, from the triangles OLK ($OL = OK$) and JLK in Fig. 6, we have

$$\sin\alpha = LK/2OK, \quad \text{and} \quad \sin\beta = LK/JK, \tag{11}$$

respectively.

By combining (10) and (11), we obtain the following:

$$\sin(\omega_0/2) = \sin\alpha/\sin\beta, \quad \alpha \le \beta \le 90°. \tag{12}$$

Thus, as β increases, ω_0 decreases (see Figs. 5*b*, *c* and *d*). It can also been seen from (12) that the value of the angle α can be determined from the slope of the straight line of the sin $(\omega_0/2)$ *vs* $1/\sin\beta$ plot. It should be noted that, for an $\{hkl\}$ family in which there is no plane at 90° from the texture axis, (12) cannot be applied since there are no hkl_0 arcs. It should also be noted that equations presented in previous work (Heidenreich, 1964; Tang & Thomas, 1993), which also relate the three angles in (12), are special cases of (12).

Now, we discuss the evolution of the arcs formed due to the intersection of the Ewald sphere with an hkl_i ($i = 1, 2, \ldots, N$ or $N-1$) spherical belt (Fig. 5 is a special case where $i = 0$, 1). A single hkl_i arc will first appear along **OF**, which is perpendicular to **OT**, when β is greater than β_i^s (Fig. 5*c*) and subsequently splits into two hkl_i arcs symmetric about the **OF** when β is greater than β_i^e (see Fig. 5*d* and also note that there is always a $-hkl_i$ arc symmetric about the origin), where

$$\beta_i^s = 90° - \eta_i - \alpha,$$

and

$$\beta_i^e = 90° - \eta_i + \alpha, \quad i = 1, 2, \ldots, N \quad \text{or} \quad N-1. \tag{13}$$

Here, β_i^s is the tilt angle where the hkl_i arc starts to appear and β_i^e is the tilt angle where the hkl_i ends as a single arc. The angle ω_{hkl_i} subtended by the single hkl_i arc can be related to β and β_i^s with the help of Fig. 7, which shows the intersection of the Ewald sphere with an hkl_i spherical belt for $\beta_i^s \le \beta \le \beta_i^e$. In Fig. 7, **OF** is the projection of **ON** on the diffraction pattern, ω_{hkl_i} is the angle subtended by the hkl_i arc with a chord of CB, which is bisected by **OF**. It follows from the triangle OCB ($OC = OB = G_{\{hkl\}}$) in Fig. 7 that

$$\cos(\omega_{hkl_i}/2) = OA/OB. \tag{14}$$

From the triangles OAD and OSD ($OS = G_{\{hkl\}}$) in Fig. 7, we also have

$$\sin\beta = OD/OA \quad \text{and} \quad \sin\beta_i^s = OD/OS, \tag{15}$$

respectively.

Consequently, this leads to

$$\cos(\omega_{hkl_i}/2) = \sin\beta_i^s/\sin\beta,$$
$$i = 1, 2, \ldots, N \quad \text{or} \quad N-1, \quad \beta_i^s \le \beta \le \beta_i^e. \tag{16}$$

From (16), it can be seen that ω_{hkl_i} increases with the tilt angle β until the hkl_i arc splits into two arcs. Since β_i^s is related to α by (13), once again we can determine α experimentally from the slope of the straight line by plotting $\cos(\omega_{hkl_i}/2)$ *vs* $1/\sin\beta$.

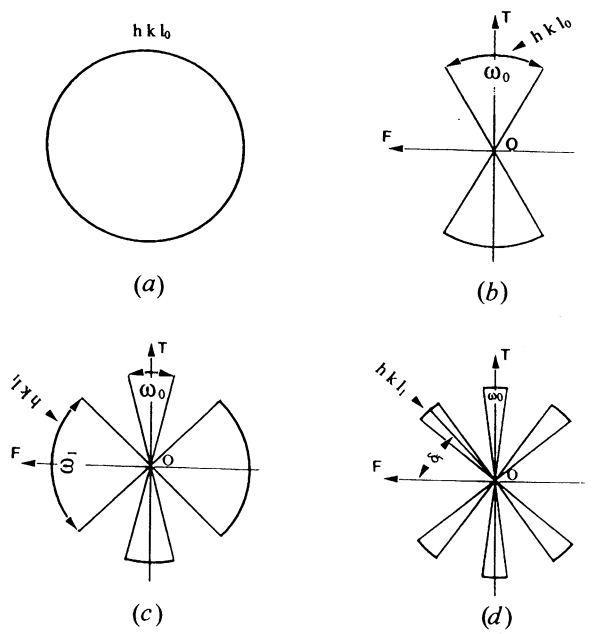

Fig. 5. Diffraction pattern evolution with tilt angle of an $\{hkl\}$ family of planes, which have to distinct angles (one is 90°) with the texture axis. (*a*) $0° \le \beta \le \alpha$, (*b*) $\alpha < \beta < \beta_1^s$, (*c*) $\beta_1^s \le \beta \le \beta_1^e$, (*d*) $\beta_1^e < \beta \le 90°$.

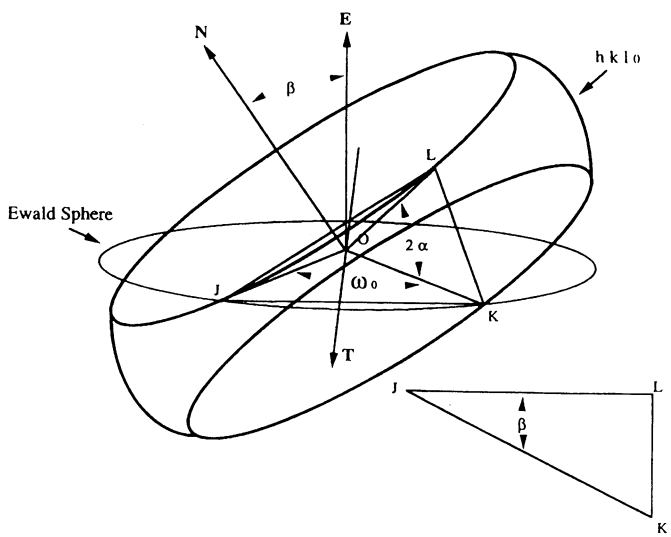

Fig. 6. Intersection of the Ewald sphere with an hkl_0 spherical belt when $\beta > \alpha$.

By combining (12) and (16), we also have

$$\sin(\omega_0/2) = \sin\alpha\cos(\omega_{hkl_i}/2)/\sin\beta_i^s,$$
$$i = 1, 2, \ldots, N \quad \text{or} \quad N-1, \quad \beta_i^s \le \beta \le \beta_i^e. \quad (17)$$

Thus, in the tilt-angle range in which (16) and (17) are valid, α can also be determined from the slope of the $\sin(\omega_0/2)$ *vs* $\cos(\omega_{hkl_i}/2)$ straight line without accurate knowledge of β. This holds for cases where hkl_0 arcs as well as hkl_0 arcs are present. When $\beta \ge \beta_i^e$, the hkl_i arc splits into two arcs that are symmetric about **OF** as shown in Fig. 5(*d*). The angle, δ_i, between the center of the arcs and **OF** is related to β and η_i as follows (Reimer, 1984):

$$\cos\eta_i = \sin\beta\cos\delta_i,$$
$$i = 1, 2, \ldots, N \quad \text{or} \quad N-1, \quad 90^\circ \ge \beta > \beta_i^e. \quad (18)$$

Thus, with the known tilt angle β and measured δ_i values, values of η_i can be calculated using (18). Then, the indices of $[uvw]$ and $[h'k'l']^*$ can be determined with the help of (1) and (4) for fibrous and lamellar textures, respectively. Examples of this are included in the second part of this paper (Tang, Feng, Lee & Laughlin, 1996).

4. Summary

The reciprocal lattice of fibrous $[uvw]$ and lamellar $[h'k'l']^*$ textured thin films consists of reciprocal circles around the texture axis. For an $\{hkl\}$ family of planes, the corresponding reciprocal circles are circles on the sphere of radius $1/d_{hkl}$. The number of the distinct reciprocal circles, N, of $\{hkl\}$ is equal to the number of distinct angles of planes in $\{hkl\}$ with the texture axis. These reciprocal circles can be in indexed hkl_i, where $i = 0, 1, 2, \ldots, N-1$ for $\{hkl\}$, in which there is at least one plane making 90° with the tilt axis and $i = 1, 2, \ldots, N$ for $\{hkl\}$, in which there are no planes making 90° with the texture axis. It has been shown that, when $[uvw]$ and $[h'k'l']^*$ have the same form, the maximum possible number, M, of distinct angles between any given $[uvw]$ direction and all planes in a given $\{hkl\}$ family is the same as that between any given $(h'k'l')$ plane and all planes in a given $\{hkl\}$ family. The values of M for all crystal systems are tabulated in Tables 1–5.

Electron diffraction patterns consist of hkl_0 rings when the electron beam is parallel to the texture axis. When the texture axis is tilted away from the electron beam about an axis in the plane of the film, electron diffraction patterns are no longer uniform rings but arcs. For diffraction arcs due to planes in an $\{hkl\}$ family, they always lie on the same circle of radius $L\lambda/d_{hkl}$. The hkl_0 arcs will always be bisected by the tilt axis. The angle ω_0 subtended by the hkl_0 arcs decreases with the tilt angle β and is related to the distribution angle α of the texture axis by (12). The hkl_i ($i = 1, 2, \ldots, N$ or $N-1$) arcs will always appear as a single arc bisected by an axis that is perpendicular to the tilt axis and eventually split into two arcs as the film is being further tilted. The angle ω_{hkl_i} subtended by the hkl_i single arc can also be related to the tilt angle β and texture axis distribution angle α through (16). By the use of (12) and (16), the α values can be determined from the slopes of the straight lines of $\sin(\omega_0/2)$ *vs* $1/\sin\beta$ and $\cos(\omega_{hkl_i}/2)$ *vs* $1/\sin\beta$ plots.

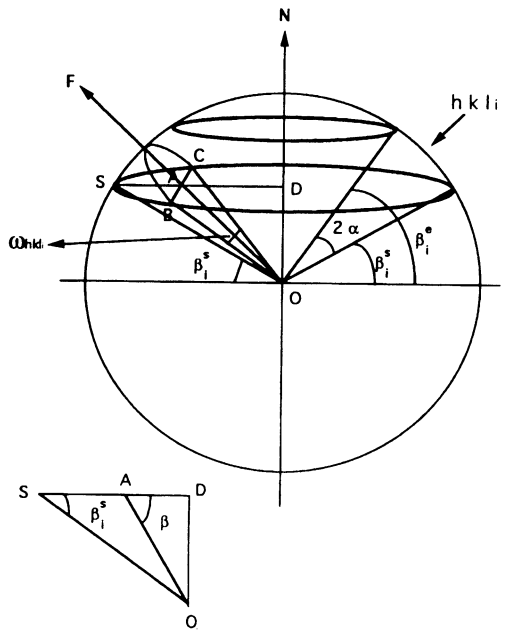

Fig. 7. Intersection of the Ewald sphere with an hkl_i spherical belt when $\beta_i^s \le \beta \le \beta_i^e$.

The authors thank Professor M. De Graef of Carnegie Mellon University for his critical reading of the manuscript. This work is supported by the National Science Foundation under grant ECD-8907068. The US government has certain rights to this material.

References

Bain, J. A., Clemens, B. M., Brennan, S. M. & Kataoka, H. (1993). *IEEE Trans. Magn.* **29**, 300–306.

Barrett, C. S. & Massalski, T. B. (1980). *Structure of Metals*, 3rd revised ed., p. 193. New York: Pergamon.

Cullity, B. D. (1978). *Elements of X-ray Diffraction*, p. 295. Reading, MA: Addison Wesley.

Feng, Y. C., Laughlin, D. E. & Lambeth, D. N. (1994). *J. Appl. Phys.* **76**, 7311–7316.

Heidenreich, R. D. (1964). *Fundamentals of Transmission Electron Microscopy*, p. 388. New York: Interscience.

Hirsch, P. B., Howie, A., Nicholson, R. B., Pashley, D. W. & Whelan, M. J. (1978). *Transmission Electron Microscopy of Thin Crystals*, 2nd ed., p. 116. Malabar, FL: Roberte E. Krieger Publishing Company.

Hono, K., Wong, B. & Laughlin, D. E. (1990). *J. Appl. Phys.* **69**, 4734–4740.

Kasper, J. S. & Lonsdale, K. (1959). *International Tables for X-ray Crystallography*, Vol. II, p. 119. Birmingham: The Kynoch Press. (Present distributor Kluwer Academic Publishers, Dordrecht.)

Reimer, L. (1984). *Transmission Electron Microscopy*, p. 407. New York: Springer.

Tang, L. & Thomas, G. (1993). *J. Appl. Phys.* **74**, 5025–5032.

Tang, L., Feng, Y. C., Lee, L.-L. & Laughlin, D. E. (1996). *J. Appl. Cryst.* **29**, 419–426.

Vainshtein, B. K. (1964). *Structure Analysis by Electron Diffraction*, p. 70. New York: Pergamon.

Zvyagin, B. B. (1992). *International Tables for Crystallography*, Vol. C, edited by A. J. C. Wilson, pp. 359–360. Dordrecht: Kluwer Academic Publishers.